Buckling patterns of graphene-boron nitride alloy on Ru(0001)

Alex Kutana[1], Andrii Goriachko[2], Zhili Hu[1], Hermann Sachdev[3], Herbert Over[4], and Boris I. Yakobson[1]

[1]*Department of Materials Science and Nanoengineering, Rice University, Houston, TX 77005*

[2]*Department of Nanophysics and Nanoelectronics, Taras Shevchenko National University of Kyiv, Glushkova Av. 4G, 03022, Kyiv, Ukraine*

[3]*Department of Inorganic Chemistry, University of Saarland, Saarbruecken, 66041 Germany*

[4] *Institute of Physical Chemistry, Justus Liebig University, Heinrich-Buff-Ring 58, Giessen, 35392 Germany*

Abstract: Buckling nano-patterns of monoatomic layer two-dimensional (2D) materials on metal substrates attract significant attention due to their rich interface morphology affecting electronic applications. We conduct an experimental-theoretical study of a 2D boron-nitrogen-carbon ($B_{x/2}N_{x/2}C_{1-x}$) alloy on Ru(0001) surface, and discover a profound relation between the composition *x* and the degree of buckling. Experimentally, we demonstrate real carbon-boron-nitrogen alloys on the Ru(0001) surface and show various morphologies of pure and mixed compounds. We further carry out density functional theory calculations using the supercells of graphene, h-BN and random BNC on Ru(0001), as well as Monte Carlo simulations for elucidating the kinetics of their growth. Our results show that unlike pure compounds (h-BN or C), the carbon-boron-nitrogen mix on Ru(0001) mostly exists in an uncorrugated form, thus greatly improving the interface contact. The likely cause of the diminished corrugation is a softening of bond angular interactions in the alloy relative to the pure phases.

Introduction

Layers of 2D materials deposited on various substrates are of great interest from both fundamental and practical points of view.[1–5] These systems are of interest because their interface physics can be utilized in new optoelectronic and spintronic devices and also because of their peculiar interface morphology. Contacts with metal surfaces can be utilized to create heterostacking photodetector devices[6] or to form a Schottky contact with a doped material by simply connecting metal electrodes.[7]

In particular, graphene (g-C) and 2D hexagonal boron nitride (h-BN) overlayers on Ru(0001) have been studied extensively, both experimentally and theoretically.[8–13] Since the first reports of graphene and BN on ruthenium, it has been shown[8,11,13,14] that characteristic Moiré patterns emerge after the deposition of pure graphene or BN on Ru(0001) due to the formation of a superstructure by the adsorbate and metal atom alignment. The corrugated BN on Ru(0001) is a proven template for metal (Au) nanoparticles formation,[15,16] which can serve as a model nano-catalytic system.[17]

On Ru(0001), the graphene-surface distance variation is typically between 2.2 and 3.7 Å,[18] and the bonding is believed to be chemical in nature,[11] while the corrugation pattern is one of the most pronounced of all metals. The interactions involve hybridization of the π states of the 2D material and *d* states of metal, and are of both covalent and noncovalent type. In graphene, hybridization results in gap opening between the π and π^* states, as local state projections show.[11–13] In terms of the substrate-adsorbate interaction strength, ruthenium belongs to the 'strong binding' metal substrate group for both graphene and BN,[18,19] although large lattice mismatch (~9%) between the hexagonal 2D adsorbate and Ru(0001) lattices prevents graphene and BN from adhering to the surface epitaxially. Instead, the mismatch in the lattice parameters of the adsorbate and underlying substrate gives rise to large-scale Moiré patterns.

Pure graphene and BN on metal surfaces reveal clear height patterns extending over large distances and traversing substrate steps when the nucleation density is low.[20] These height patterns have been studied with DFT calculations on Ru(0001)[13] and other transition metals.[12,19,21] Since metal *d* bands play an important role in the adhesive interactions, the interaction strength changes with varying metal species.[22] Previously, the interaction strength of graphene with the Ru(0001) has been fine-tuned by changing the surface composition through alloying of Ru with Pt.[23] In this work, we study the change in interactions by varying the species of the adsorbate itself, by using the 2D BNC alloy, while keeping the Ru(0001) substrate composition constant. Alloying C and BN into 2D BNC can be attractive from a practical point of view due to wide modulation of key properties such as electronic band gaps.[24] The synthesized single-layer BNC alloys on Ru(0001) have been first reported by us[16] and their utility in formation of nano-patterns has been discussed. Subsequently, other techniques for producing macroscopic quantities of BNC have been proposed.[25] Here we examine the mixing at the atomic scale and establish the connection between the local atomic configurations in an alloy and resulting nanoscale patterns.

Methods

Total energies and Hellmann-Feynman forces on ions were calculated with density functional theory (DFT), within the local density approximation (LDA) to exchange-correlation potential, and utilizing projector-augmented-wave (PAW) pseudopotentials to represent core electrons, as implemented in VASP.[26] The kinetic energy cutoff for the plane-wave basis was set to 400 eV in all calculations, and spin-orbit interactions were neglected. In all calculations with large supercells only the Γ point was sampled, and atoms were relaxed until the maximum force on any unconstrained atom was less than 0.05 eV/Å. The Ru(0001) surface was represented by two periodic layers of Ru atoms, with the bottom layer fixed. For graphene on Ru(0001), an 11(C):10(Ru) coincidence site lattice was used, whereas 14(BN):13(Ru) and 14($B_{1/4}N_{1/4}C_{1/2}$):13(Ru) coincidence site lattices were used for Ru-deposited BN and BNC, respectively. Monte Carlo simulations of BN growth by substitution in graphene were carried out using a dynamic scheme, where each trial substitutional move was either accepted or rejected with the probability that is determined by the value of the reaction energy barrier.

Theoretical results and discussion

Ab initio calculations of 2D overlayers on Ru(0001) The two-dimensional hexagonal lattices of the Ru(0001) surface and graphene or BN layers were rotationally oriented the same way, so that all of their in-plane directions are parallel. Other layer orientations were not considered in this work due to computational constraints on the system size, although the rotational degree of freedom may play role in these systems. In the supercell calculations, varied interlayer registries in the supercell give rise to Moiré patterns and periodic height profiles. We used a 11(C):10(Ru) coincidence site lattice for graphene on Ru(0001); similar height profiles are obtained with a 12(C):11(Ru) lattice. The obtained height profile of graphene on Ru(0001) is shown in Figure 1a. It displays the well-familiar periodic valleys and elevations that is observed by us experimentally, as well as reported in the earlier experiments and calculations.[13,27–29] Various interlayer registries are reproduced locally: any of the two C atoms in the graphene unit cell positioned directly above a first-layer metal atom (top site) yield attractive interactions, resulting in depressions (valleys) of the height profile of the graphene film. When both C atoms are at the hollow sites (fcc and hcp), the outcome is net repulsion, resulting in elevations. The correspondence between the local layer stacking and height is visible more clearly in Figure 1d, where the height of carbon atoms is shown with color. The difference in height between valleys and elevations is ~0.15 nm, in good agreement with our measurements on C/Ru(0001).

For BN on Ru(0001), a 14(BN):13(Ru) coincidence lattice was used. The results of geometry optimization for BN are shown in Figure 1b, agreeing well with our experimental results, as well as previous findings[11,13] and with theory.[19,21] In case of deposited BN, unlike graphene, where any of the two C atoms positioned directly above a top site yield attractive interactions, net attraction results only when N atoms are positioned at the top site, but B atoms interact with the top site repulsively. At the hollow fcc and hcp sites, the net repulsion results for both B and N atoms in BN. Just as the pattern of valleys and elevations for graphene-Ru(0001), the nanomesh pattern observed for BN-Ru(0001)[9] is a purely geometrical consequence of these local interactions.

Unlike pure graphene or BN, there are less spatial correlations among atomic species occupying lattice sites in a random BNC alloy, which would lead to a less corrugated height profile. To test this assumption, we carried out a calculation using a quasi-random BNC structure, in which half of C_2 dimers in graphene are substituted with BN dimers. (We note that removal of a C_2 dimer costs actually less energy than for a C monomer.[30]) A much flatter profile is indeed obtained, as shown in Figure 1c. In this structure, height variations are much more subdued compared to either graphene or BN, but still present because of the local ordering effects. These calculations agree well with the experimental STM profiles for the BNC alloy discussed below. The mixed BNC layer is closer to the metal surface than either graphene or BN, with an average distance to the top layer of Ru atoms being 2.41 Å, compared with average distances of 2.49 Å and 2.60 Å, for graphene and BN, respectively. All three systems have approximately same height differences of ~1.5 Å between the lowest and highest points, but BNC is on average flatter, with a standard deviation of 0.38 Å, compared with values of 0.44 Å and 0.52 Å for graphene and BN, respectively. We thus obtain a clear direct theoretical confirmation of the flattening of the height profile and disappearance of corrugations in the single-layer BNC alloy on Ru(0001) using DFT calculations. Since it is evident from the potential curves in Figure S1 that the interaction between the overlayer atoms and substrate are sharply divided into two classes – ones with a potential minimum and ones that are purely repulsive – it is natural to expect a more flat profile in a randomly mixed compound compared to pure graphene or BN.

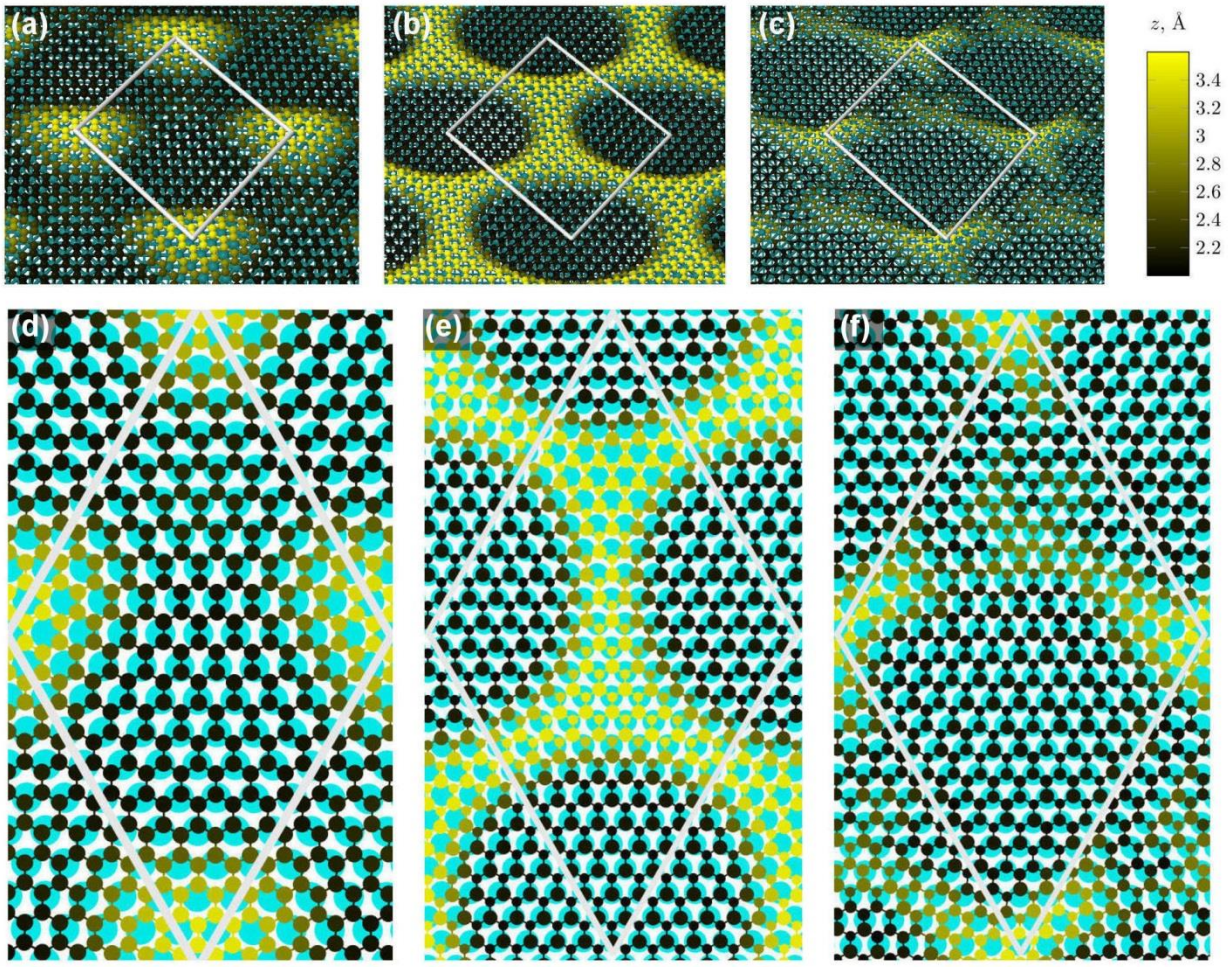

Figure 1 (color online). Height profiles and stacking of (a) graphene, (b) BN nanomesh, and (c) BNC random alloy on Ru(0001), obtained with DFT calculations. Coincidence site lattices were (a) 11(C):10(Ru), (b) 14(BN):13(Ru), and (c) 14(BNC):13(Ru). Unit cells are shown for each system. The height *z* is the normal distance to the average plane of the first layer of Ru atoms. (d)-(f) Top view of the same structures. Atom types in (e), (f) are encoded by circle size: B-small, C-medium, N-large. For clarity, only the first layer of Ru atoms is shown.

However, there is another possible explanation of the profile flattening in BNC, namely softening of angular interactions on going from the pure compounds to the BNC alloy. Figure 2 shows calculated normalized distributions of bond angles in g-C, BN, and BNC on Ru(0001). Graphene displays the narrowest distribution, followed closely by that of BN, with distribution for BNC being much wider. The local angular distortions observed in BNC help avoid unfavorable stacking configurations. For example, for carbon and nitrogen atoms occupying energetically unfavorable positions, bond angle distortions can be utilized to shifts these atoms towards the top sites on Ru(0001), helping to minimize the total energy and at the same time decreasing the distance to the substrate. This would lead to a flatter profile in the

BNC alloy, as compared to g-C and BN where there are highly directional sp^2-bonds. So far we have considered only a single BNC CSL that was taken to be same as in one of the pure compounds, thus ignoring possible effects of incommensuration on the height profile. However, it could be possible that such effects play an important role, and thus should be examined more carefully in the future work.

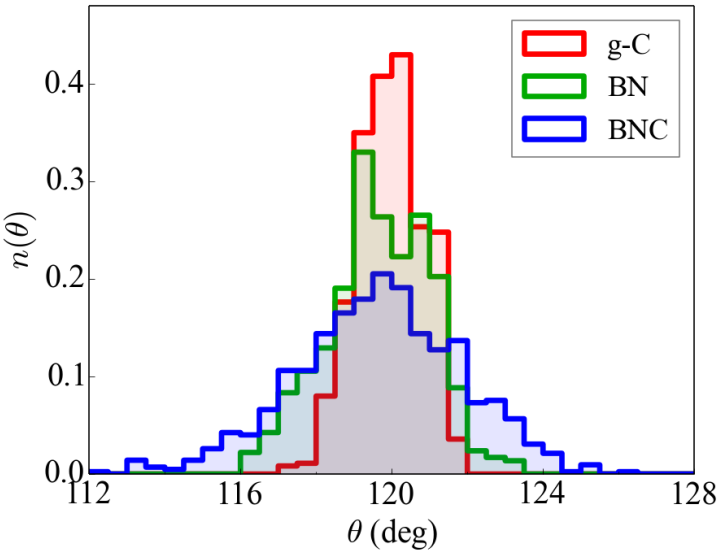

Figure 2 (color online). Calculated normalized distributions of bond angles in g-C, BN, and random BNC alloy on Ru(0001).

Kinetic Monte Carlo calculations In order to get insights into the dynamics of carbon-boron-nitrogen mixture formation, we have carried out kinetic Monte Carlo (MC) simulations of BN substitution of graphene lattice on the Ru(0001) surface. The simulations took place on a 50×30 honeycomb graphene-like lattice. Initially, the lattice is filled with carbon atoms producing a graphene sheet with the total of 6000 lattice atoms. The lattice atoms are replaced by boron-nitrogen atom pairs with a specific probability rate. The rate for the lattice atom substitution depends on the activation energy according to the Arrhenius equation:

$$k = Ae^{-E_a/(k_B T)} \tag{1}$$

where k is the chemical reaction rate constant, T is the temperature, A is the prefactor, E_a is the activation energy for the substitution of BN pair, and k_B=1.38×10^{-23} J/K is the Boltzmann constant. The activation energy E_a depends on the environment of the reacting atom. For example, if all of the neighboring atoms are carbons, then the value of E_a should be larger compared with the case when some of the neighboring atoms are borons or nitrogens. The higher the E_a the lower is the probability for substitution. The exact values of reaction barriers E_a for various kinds of neighboring environments are difficult to calculate and currently not known. To obtain the best guess for the reaction barriers, we adopted the Bell–Evans–Polanyi (BEP) principle. The BEP principle states that the difference in activation energies between two

related reactions is proportional to the difference of their reaction enthalpies. This relationship can be expressed as:

$$E_a = E_r + \alpha \Delta H \tag{2}$$

where E_r is the inherent activation energy of this type of reaction, ΔH is the enthalpy of reaction, and $\alpha \in [0,1]$ characterizes the position of the transition state along the reaction coordinate. For the current process, E_r is the energy change upon substituting a BN pair into an all-carbon structure. In what follows, E_r=0 and α=0.5 is adopted, and ΔH is estimated as the conformation energy of BN pair or BB/NN pair by density functional theory DFT. The values are calculated to be E_{BN}=0.539 eV and $E_{BB/NN}$=1.758 eV for BN pair and BB/NN pair, respectively, using 2×1 cells in vacuum. ΔH is then evaluated as $\Delta H = N_{BN}E_{BN} + N_{BB/NN}E_{BB/NN}$, where N_{BN} is the number of BN bonds to be formed and $N_{BB/NN}$ is the number of BB/NN bonds to be formed, after the substitution of a CC pair with a BN pair. Practically, due to the large difference between E_{BN} and $E_{BB/NN}$, the rate for the formation of BB or NN bonds was set to 0 in the simulation.

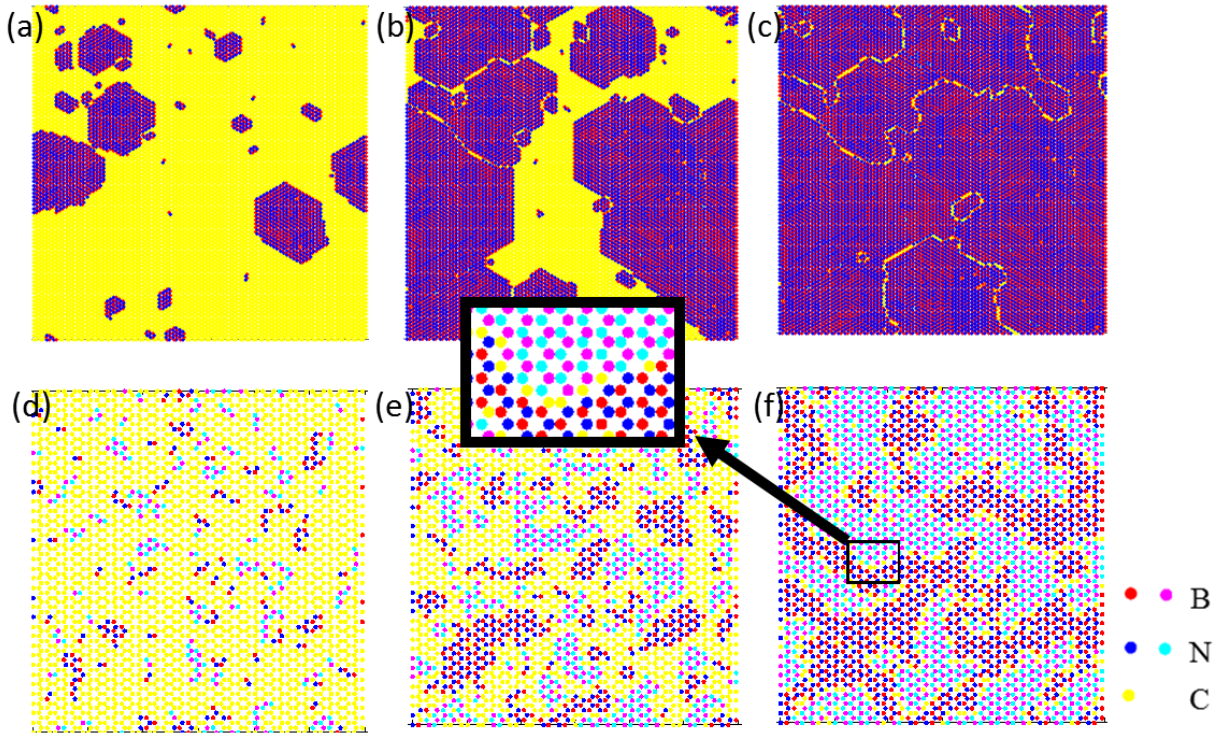

Figure 3 (color online). Time series of a Monte Carlo simulation of BN growth by dimer substitution in graphene on Ru(0001) (a-c) at T=500 K and (d-f) at T=1200 K. Inset shows the enlarged view of the carbon-chain domain wall. Red and magenta circles represent B atoms belonging to different islands, blue and cyan circles represent N atoms from different islands, and yellow circles represent carbon atom.

The simulation was implemented in Matlab and the dynamics of substitutions was followed. The time sequence for substitutions at T=500 K is shown in Figures 3a-c. The initial growth stage can be observed in Figure 3a, where random seeds appear and grow into hexagon-like shapes. Gradually some grains

become too large to be separated, so that they will either fuse into bigger grains or form domain walls as seen in Figure 3b. At this stage, in-plane interfaces between graphene and BN are formed.[31] Finally, Figure 3c shows that at the end of the simulation BN grains with carbon boundaries as domain walls remain. An analysis shows that this is due to the fact that by the process of substitution of CC pairs with BN pairs, the formation of BB or NN bonds as the domain wall becomes inevitable (see inset in Figure 3), therefore greatly decreasing the reaction rate.

It would be of interest to predict the number of carbon atoms at the boundaries as a function of temperature. The simulation results are shown in Figure 4, where it is seen that at low temperatures the number of carbon atoms remaining at the boundary is small and increases with increasing temperature. We have also performed an extra analytical analysis beyond the MC calculation results shown in Figure 4. We base our low-temperature analysis on the observation from the simulation, that the grain growth mostly occurs by addition of only one BN bond (N_{BN}=1). The occurrence with N_{BN}>1 is rare assuming the grains to be sparse at low temperatures, thus unimportant. Physically, $\Delta H_1=\Delta H(N_{BN}=1)$ defines the speed of BN grain growth normal to its edge, if grain seeds form at the constant rate $v=\exp(-\alpha\Delta H_1/k_BT)$. Apparently, the seed formation rate is proportional to the area of the simulation canvas. When scaling the canvas by L times while enlarging v by L^3 times, the evolution profile of BN grains is not changed. This gives the following scaling law:

$$r_c = cv^{1/3} = ce^{-\frac{\alpha\Delta H}{3k_BT}} \tag{3}$$

where r_c is the fraction of carbon atoms remaining at the boundaries, c is a constant that could be fitted to experiment or simulation data.

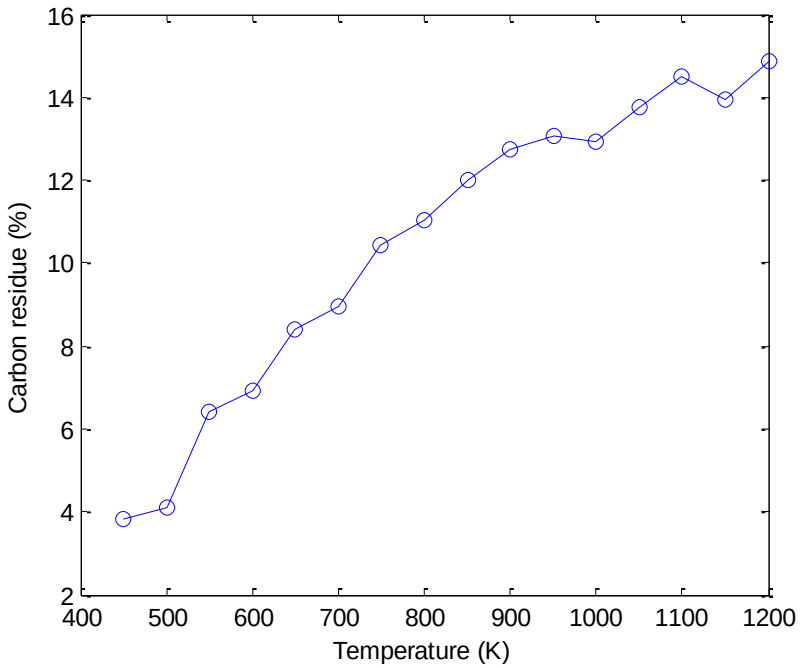

Figure 4 Fraction of carbon atoms remaining at the boundary after completion of the growth of BN grains as a function of temperature.

Systems with a lattice mismatch such as the 2D adsorbate-metal substrate arrangements studied here as well as related vertically stacked van der Waals heterostructures[32] present an intriguing subject. One of the open questions for these systems is whether the periodic models used in DFT calculations give adequate description of their incommensurate lattices and corresponding electronic structures. One may expect that periodic boundary conditions that are normally used in crystal calculations may not be adequate for systems near phase transitions between commensurate and incommensurate structures. For systems near such transition, there could be great sensitivity to a particular CSL used in a calculation. A careful examination of the suitability of the periodic boundary conditions would be necessary in such case. A somewhat related issue is the accuracy of density functionals employed for van der Waals solids and weakly bound 2D structures on metal surfaces. Similar to the choice of the CSL discussed above, a particular density functional being used may affect the results. In large systems with weak interactions (like the van der Waals), the structure may undergo large geometrical distortions and/or electronic structure change. In addition, while the use of the CSL may help eliminate the total strain, local strains within the supercell must be reproduced by the functional as well. More accurate electronic structure methods that eliminate density functional dependence may be necessary in such cases. Ideally, one should be able to quantify the uncertainties and obtain systematic estimates of the method errors – a requirement that is hard to realize within the density functional theory due to its non-prescriptive nature. While hybrid functionals and post-DFT perturbative corrections such as the GW method give some improvements over the standard DFT results, there are still no reliable ways of estimating accuracy. LDA is known to yield reasonable geometries and sometimes binding energies in many systems with van der Waals bonding, but conceptually, there is no good reason for this method to work well in these systems. Thus, good agreement provided by the method is probably fortuitous and related to the well-known overbinding of LDA. For a better theoretical foundation, one needs to apply nonlocal functionals accounting van der Waals interactions, such as the vdW-DF functional.[33] Such functionals most likely give improved accuracy for 2D systems on transition metals,[34,35] although reliable experimental validations of their superior performance are difficult to carry out.

Finally, if one wishes to achieve similar level of accuracy for kinetic processes as one typically has in static calculations, long time scales must be accessed. Since spanning the necessary time scales is almost impossible with the standard DFT, some coarse-grained models must be employed. Linking the microscopic (DFT) and mesoscopic (kinetic MC) regimes and the corresponding length and time scales in a model that goes beyond the simple Arrhenius formalism is still an issue in such dynamic systems that should be addressed in the future.

Experimental results

The experimental section of our work was aimed at demonstration of real carbon-boron-nitrogen alloys on the Ru(0001) surface and investigation of their topography by means of scanning tunneling microscopy (STM).

The basic pattern of the h-BN/Ru(0001) nanomesh is a hexagonal array of depressions (further called pores), as can be seen, for example, in the upper part of the STM image in Figure 5a. One can deduce the array's periodicity of ~3.33 nm and the depth of the pore relative to the surrounding of ~0.08 nm from the

corresponding height-distance cross-section. Circular pores (Ø ~ 2 nm) (depressions), similar to the one marked by "p" in Figure 5a, are essentially regular corrugation features of the h-BN layer, of which the nanomesh consists of. The depth of the pore is actually a magnitude of the h-BN's layer corrugation, due to interaction with the Ru(0001) substrate. Areas of the h-BN layer, which are higher than the pores (designated by "w"), are referred to as "wires" (elevations) creating a visual perception of the mesh in the STM images. According to our theoretical model (Figure 1b) and the previous works of other authors,[13] the pores are parts of the h-BN layer with N atoms occupying on-top positions on Ru(0001), while the wires are formed by parts of the layer with N atoms in the fcc or hcp positions.

A close inspection of Figure 5a also reveals numerous deviations from the ideal coincidence lattice. In the first place, the nanomesh pattern is interrupted at single atomic steps of the metallic substrate (marked by "s"). We observe a specific registry of the pattern across the step with the clear alignment of adjacent pores on the upper and lower terraces.

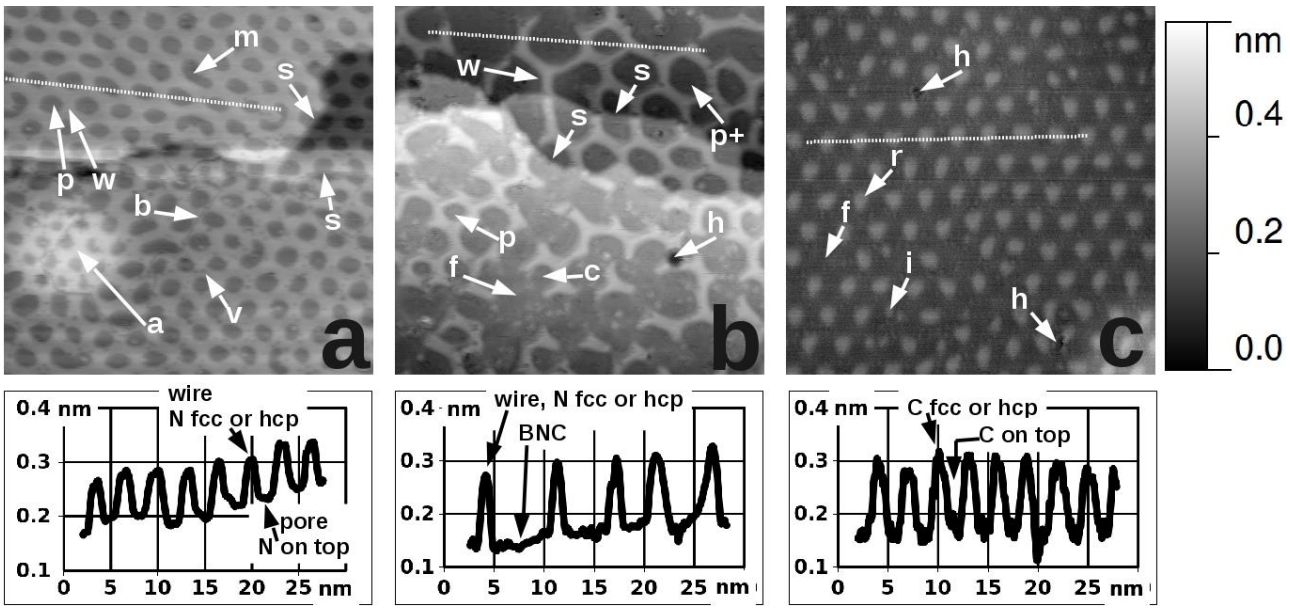

Figure 5. STM images from BN to C on Ru(0001). (a) h-BN/Ru(0001), sample bias voltage 2V, tunneling current 1 nA; (b) BNC/Ru(0001), 2V, 1nA; (c) C/Ru(0001), 0.4 V, 4.5 nA. All images are 34 nm × 34 nm in size. The grey scale corresponds to 0.6 nm height span. Below the images are height-distance cross-sections taken along the corresponding hatched lines. Any non-zero slope of the cross-section as a whole is due to incomplete background subtraction on the given particular terrace of the sample. Characteristic features on the images are marked as following: a - area above the buried Ar bubble; b - domain boundary; c - cavity (partially enclosed pore); f - flat “uncorrugated” area; h - hole (discontinuity) in the deposited layer; i - irregular non-periodic corrugation; m - merger of two pores; p - standard pore (height depression) in the deposited layer; p+ - enlarged pore (diameter larger than standard); r - regular periodic corrugation; s - monoatomic substrate step; v - atomic size vacancy.

Other common irregularities of the nanomesh pattern are substantial variations in pore diameter and lateral periodicity. A distinct type of irregularity is a merger of two pores into a single one (designated by "m") also leading to disruptions of hexagonal order. There are numerous discontinuities in the h-BN layer, coming in the form of domain boundaries along arbitrarily shaped curves (designated by "b") or vacancies of atomic size (designated by “v”). In the lower left quarter of Figure 5a, we observe a large scale

elevation of circular shape (designated by "a"), spanning several nanomesh periods, which is attributed to the trapped Ar bubble beneath the surface. Such "underground" bubbles originate from the ion sputtering procedure during surface preparation and could not be avoided.[36] The Ar atoms are trapped below the surface and form clusters, thus causing a local expansion of the substrate's atomic lattice reaching out to the surface in the form of a hill. As a result, there is a specific distortion of the nanomesh pattern above such a hill, namely, both the pore's diameter and the pattern's periodicity are decreased. Simultaneously, we observe elongation of the pores, situated along the hill's perimeter, towards its center.

Our experimental observation of the 3.33 nm h-BN/Ru(0001) superstructure periodicity is somewhat lower than the expected value of 3.52 nm from our simulated 14(BN):13(Ru) coincidence lattice (Figures 1b,e). This discrepancy may stem from the presence of various irregularities of the superstructure, which are intrinsic in their nature, as they were observed for every sample preparation in numerous experimental attempts and also on different single crystal Ru(0001) substrates. In this respect the h-BN/Ru(0001) superstructure is substantially different from the closely related 13(BN):12Ru h-BN/Rh(111) superstructure where long range order is evident. It seems reasonable, that the 14(BN):13(Ru) unit cell of the superstructure is an ideal lowest energy structure, which is never realized in its exact form. Instead, numerous defects and deviations from ideal hexagonal superlattice decrease the actual periodicity of the real superstructure.

In order to produce a carbon-boron-nitrogen alloy, we have chosen a N,N,N-trimethylborazine precursor ($B_3C_3N_3H_{12}$), mainly because of its similarity to borazine. Both of them are liquid at room temperature and their vapors could be easily dosed to the sample by regulating a variable leak valve between the precursor container vessel and the sample preparation ultra-high vacuum chamber. In this way, only the precursor liquid had to be changed in the container vessel, while the preparation procedure and the experimental set up remained otherwise unaltered. In Figure 5b we present the STM image of the surface superstructure obtained with $B_3C_3N_3H_{12}$.

The pattern formed by the carbon-boron-nitrogen alloy on Ru(0001) consists of two distinct height levels: a lower level (features "p", "p+", "c" and "f") and a higher level ("w" features) with ~ 0.12 nm difference between them. A limited number of holes "h" were also found within the carbon-boron-nitrogen layer. In some locations we observe round pores "p" surrounded by wires, as inherent to the h-BN/Ru(0001) nanomesh. Generally, however, the wires' pattern is irregular, producing pores of increased diameter "p+", partially enclosed cavities "c" and almost flat areas "f" of ~10 nm in lateral size. It is clearly seen that the h-BN layer's height is the same within the pores, cavities and extended uncorrugated areas.

Our ab initio calculation results (Figure 1) indicate the same height of ~ 0.2 nm above the Ru(0001) substrate of both the pore regions of the pure h-BN layer (Figure 1b) and the fully mixed BNC layer in almost every location except for small ripples (Figure 1c). Therefore, it seems plausible to assign the areas of type "f" to those covered by the BNC alloy. Furthermore, a combination of such BNC patches with BN type features ("p", "c" and "w") in Figure 5b could have been enforced by the trimethylborazine precursor's stoichiometry, which has a surplus of BN relative to the BNC alloy. Also, the "p+" pores can be explained by the BNC areas of corresponding sizes trapped inside the closed contours of the BN wires "w". At this stage, our general conclusion is that any uncorrugated area with lateral size larger than the standard 2 nm pore of BN nanomesh is attributed to the patch of BNC/Ru(0001).

In order to cover the entire range of nanostructuring types on the $B_{x/2}N_{x/2}C_{1-x}$ axis, we also demonstrate the superstructure formed by pure graphene (g-C) on Ru(0001). The g-C/Ru(0001) was reported by Wintterlin *et al.*[27] and Hong-Jun *et al.*[28] after annealing single crystal Ru(0001) samples in

ultra-high vacuum. Carbon impurities were segregating from the bulk of the ruthenium sample to its surface, forming a graphene layer on top of it. In order to reproduce these results we have changed only the final step of our preparation procedures for depositing BN and BNC layers. Namely, the flux of any precursor to the surface was completely eliminated, while all other aspects of the preparation procedure remained unchanged. As a result, graphene patches have appeared on the substrate, as shown in Figure 5c. On top of Ru(0001), graphene forms a superstructure in the form of regular elevations (designated by "r") arranged in a hexagonal array with ~ 3.0 nm periodicity. This value is in line with previous experimental observations of other authors[27,28,37,38] as well as with the expected value of 2.98 nm for the 12(g-C):11(Ru) superstructure (Figure 1a). On the real surface, this ideal hexagonal superstructure is disturbed by carbon layer discontinuities (holes marked "h"), single absent elevations (flat supercell units marked "f") as well as irregularly placed and shaped elevations (marked "i"). Since no boron and no nitrogen were supplied to the sample in this experiment, we believe that "f" features in Figure 5c are not due to boron-carbon-nitrogen alloy. We speculate that the "f" and "i" features in Figure 5c are distortions of the ideal hexagonal superstructure due to various defects in the metal substrate and the graphene overlayer as well as their alignment relative to each other.

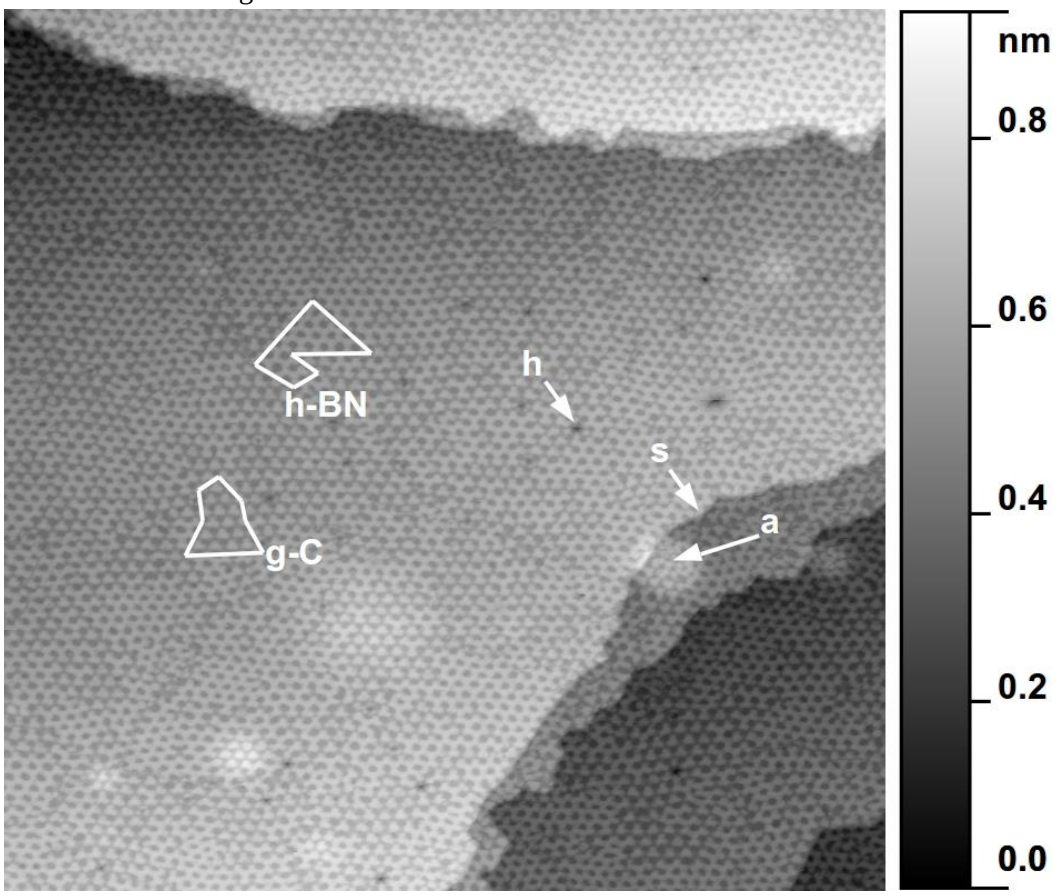

Figure 6. STM image of h-BN and g-C patches on Ru(0001). Image size: 172 nm × 172 nm; sample bias voltage 2V, tunneling current 1 nA; Two different patches of graphene and boron nitride are outlined in white and marked accordingly. Selected individual features are designated similar as in Figure 5: a - area above the buried Ar bubble; h - hole (discontinuity) in the deposited layer; s - monoatomic substrate step.

Three cases depicted in Figure 5 do not exhaust all types of morphologies formed by BN and C on Ru(0001). In Figure 6 we show a large scale STM image of what we identify as a partially failed attempt to deposit the pure BN film. The specifics of the borazine precursor is its tendency to polymerize into BN with hydrogen release, which is an autocatalytic reaction. For the preparation procedure described above, the vapors of the freshly synthesized borazine liquid produces the morphology shown in Figure 5a. If the same deposition procedure is repeated after several weeks of keeping the precursor container vessel at room temperature, the resulting morphology is shown in Figure 6. In this case the surface is covered by a mixture of patches, some of them resembling the h-BN/Ru(0001) in Figure 5a, while others resembling the g-C/Ru(0001) in Figure 5c.

A plausible explanation for the result in Figure 6 is that the nominal vapor pressure of 3×10^{-7} mbar does not entirely correspond to borazine molecules during deposition. When the liquid precursor is partially polymerized, not enough borazine molecules are available to evaporate into vacuum when the variable leak valve is opened into the preparation chamber. In our experimental setup, the valve is opened until the total nominal pressure is reached regardless by which molecular species it is created. Therefore, if borazine molecules were scarce, the rest was made up by outgassing from the walls of the container vessel and the tubing of the gas line. In such conditions, not enough boron nitride was supplied to the surface in order to complete a single monolayer. Thus, carbon diffusing from the bulk of ruthenium and also being present in the outgassing species has formed graphene patches where the substrate was not covered by h-BN. In contrast to atomic level BNC alloys in selected areas of Figure 5b, the present case appears to be a mixture between BN and C on a much rougher lateral scale (~ 10 nm, or several superstructure unit cells).

Conclusion

In conclusion, we examined theoretically and experimentally the structure, energetics, and kinetics of formation of two-dimensional carbon, BN, and boron-nitrogen-carbon alloys on Ru(0001). In both experiment and theory, we find that the 2D BNC alloy interacts differently with the substrate than either pure graphene or BN. In particular, the regular height corrugations associated with the Moiré patterns are much less pronounced in the BNC alloy. We attribute this difference to the softening of the angular interactions of the sp^2 network in the alloy, allowing for a more facile adjustment to the substrate. As a result, the overall adsorbate-substrate distance decreases. In addition to homogeneous BNC phase, we also observe regions of phase separated BN and g-C domains with grain boundaries, and their appearance and growth is studied with Monte Carlo calculations.

Appendix

Registry-dependent interactions of individual atoms. Before considering large supercells with realistic coincidence site lattices (CSL), we also examined the interaction of 2D C and BN with the Ru(0001) surface in a simple 1×1 unit cell to gain understanding of the local substrate-adsorbate interactions. In-plane deformations resulting from the lattice mismatch between the 2D material and metal surface are of little consequence for the qualitative picture given below. For a material with a honeycomb structure such as graphene, the following high-symmetry arrangements exist on the equilateral triangular Ru(0001) lattice: (1) half of C atoms are above one type of hollow cites (fcc or hcp) while the other half are above the top sites, and (2) half of C atoms are above one type of hollow cites while the other half are above the other type. Figure S1 shows the calculated interaction energies as a function of the graphene layer vertical

position *z* for these two cases in a 1×1 cell, where both the 2D layer and Ru(0001) surface are flat, and all atom coordinates held fixed. It is clear that the interactions of C in graphene with Ru(0001) are strongly registry-dependent: the interactions of C atoms directly above Ru atoms are attractive with a well-pronounced energy minimum, whereas the interactions at the hollow sites are mostly repulsive with a very shallow local minimum, as shown in Figure S1a. This leads to a strong preference for the C atoms to be at the top site. In case of BN, only interactions with N at the top site are attractive, as seen in Figure S1b; for other positions (top B, hollow N, and hollow B) the interactions are repulsive. In the actual CSL, these registries are reproduced locally, giving rise to the height profiles observed in our STM measurements.

Acknowledgement

Work at Rice was supported by the U.S. Army Research Office MURI Grant W911NF-11-1-0362.

References

[1] W. A. de Heer, C. Berger, X. Wu, P. N. First, E. H. Conrad, X. Li, T. Li, M. Sprinkle, J. Hass, M. L. Sadowski, M. Potemski, G. Martinez, *Solid State Commun.* **2007**, *143*, 92.

[2] M. J. Allen, V. C. Tung, R. B. Kaner, *Chem. Rev.* **2010**, *110*, 132.

[3] K. S. Kim, Y. Zhao, H. Jang, S. Y. Lee, J. M. Kim, K. S. Kim, J.-H. Ahn, P. Kim, J.-Y. Choi, B. H. Hong, *Nature* **2009**, *457*, 706.

[4] L. Song, L. Ci, H. Lu, P. B. Sorokin, C. Jin, J. Ni, A. G. Kvashnin, D. G. Kvashnin, J. Lou, B. I. Yakobson, P. M. Ajayan, *Nano Lett.* **2010**, *10*, 3209.

[5] J. V. Barth, G. Costantini, K. Kern, *Nature* **2005**, *437*, 671.

[6] P. Avouris, *Nano Lett.* **2010**, *10*, 4285.

[7] G. Giovannetti, P. A. Khomyakov, G. Brocks, V. M. Karpan, J. van den Brink, P. J. Kelly, *Phys Rev Lett* **2008**, *101*, 026803.

[8] P. W. Sutter, J.-I. Flege, E. A. Sutter, *Nat Mater* **2008**, *7*, 406.

[9] A. Goriachko, He, M. Knapp, H. Over, M. Corso, T. Brugger, S. Berner, J. Osterwalder, T. Greber, *Langmuir* **2007**, *23*, 2928.

[10] S. Berner, M. Corso, R. Widmer, O. Groening, R. Laskowski, P. Blaha, K. Schwarz, A. Goriachko, H. Over, S. Gsell, M. Schreck, H. Sachdev, T. Greber, J. Osterwalder, *Angew. Chem. Int. Ed.* **2007**, *46*, 5115.

[11] B. Wang, M.-L. Bocquet, S. Marchini, S. Günther, J. Wintterlin, *Phys. Chem. Chem. Phys.* **2008**, *10*, 3530.

[12] M. Iannuzzi, J. Hutter, *Surf. Sci.* **2011**, *605*, 1360.

[13] T. Brugger, S. Günther, B. Wang, J. H. Dil, M.-L. Bocquet, J. Osterwalder, J. Wintterlin, T. Greber, *Phys. Rev. B* **2009**, *79*, 045407.

[14] M. Corso, *Science* **2004**, *303*, 217.

[15] A. Goriachko, Y. B. He, H. Over, *J. Phys. Chem. C* **2008**, *112*, 8147.

[16] A. Goriachko, H. Over, *Z. Für Phys. Chem.* **2009**, *223*, 157.

[17] A. Goriachko, A. A. Zakharov, H. Over, *J. Phys. Chem. C* **2008**, *112*, 10423.

[18] J. Wintterlin, M.-L. Bocquet, *Surf. Sci.* **2009**, *603*, 1841.

[19] R. Laskowski, P. Blaha, *Phys Rev B* **2010**, *81*, 075418.

[20] J. Lu, P. S. E. Yeo, Y. Zheng, H. Xu, C. K. Gan, M. B. Sullivan, A. H. Castro Neto, K. P. Loh, *J. Am. Chem. Soc.* **2013**, *135*, 2368.

[21] J. Gómez Díaz, Y. Ding, R. Koitz, A. Seitsonen, M. Iannuzzi, J. Hutter, *Theor. Chem. Acc.* **2013**, *132*, DOI 10.1007/s00214-013-1350-z.

[22] A. B. Preobrajenski, M. L. Ng, A. S. Vinogradov, N. M\aartensson, *Phys Rev B* **2008**, *78*, 073401.

[23] D. Alfe, M. Pozzo, E. Miniussi, S. Gunther, P. Lacovig, S. Lizzit, R. Larciprete, B. S. Burgos, T. O. Mentes, A. Locatelli, A. Baraldi, *Sci Rep* **2013**, *3*, 2430.

[24] M. Zhang, G. Gao, A. Kutana, Y. Wang, X. Zou, J. S. Tse, B. I. Yakobson, H. Li, H. Liu, Y. Ma, *Nanoscale* **2015**, *7*, 12023.

[25] X. Wang, C. Zhi, L. Li, H. Zeng, C. Li, M. Mitome, D. Golberg, Y. Bando, *Adv. Mater.* **2011**, *23*, 4072.

[26] G. Kresse, J. Furthmüller, *Phys Rev B* **1996**, *54*, 11169.

[27] S. Marchini, S. Günther, J. Wintterlin, *Phys Rev B* **2007**, *76*, 075429.

[28] P. Yi, S. Dong-Xia, G. Hong-Jun, *Chin. Phys.* **2007**, *16*, 3151.

[29] B. Wang, S. Günther, J. Wintterlin, M.-L. Bocquet, *New J. Phys.* **2010**, *12*, 043041.

[30] J. Y. Huang, F. Ding, K. Jiao, B. I. Yakobson, *Phys Rev Lett* **2007**, *99*, 175503.

[31] Z. Liu, L. Ma, G. Shi, W. Zhou, Y. Gong, S. Lei, X. Yang, J. Zhang, J. Yu, K. P. Hackenberg, A. Babakhani, J.-C. Idrobo, R. Vajtai, J. Lou, P. M. Ajayan, *Nat Nano* **2013**, *8*, 119.

[32] C. R. Woods, L. Britnell, A. Eckmann, R. S. Ma, J. C. Lu, H. M. Guo, X. Lin, G. L. Yu, Y. Cao, R. V. Gorbachev, A. V. Kretinin, J. Park, L. A. Ponomarenko, M. I. Katsnelson, Y. N. Gornostyrev, K. Watanabe, T. Taniguchi, C. Casiraghi, H.-J. Gao, A. K. Geim, K. S. Novoselov, *Nat Phys* **2014**, *10*, 451.

[33] M. Dion, H. Rydberg, E. Schröder, D. C. Langreth, B. I. Lundqvist, *Phys Rev Lett* **2004**, *92*, 246401.

[34] C. Busse, P. Lazić, R. Djemour, J. Coraux, T. Gerber, N. Atodiresei, V. Caciuc, R. Brako, A. T. N'Diaye, S. Blügel, J. Zegenhagen, T. Michely, *Phys Rev Lett* **2011**, *107*, 036101.

[35] M. Bokdam, G. Brocks, M. I. Katsnelson, P. J. Kelly, *Phys Rev B* **2014**, *90*, 085415.

[36] M. Gsell, P. Jakob, D. Menzel, *Science* **1998**, *280*, 717.

[37] A. L. Vázquez de Parga, F. Calleja, B. Borca, M. C. G. Passeggi, J. J. Hinarejos, F. Guinea, R. Miranda, *Phys Rev Lett* **2008**, *100*, 056807.

[38] M.-C. Wu, Q. Xu, D. W. Goodman, *J. Phys. Chem.* **1994**, *98*, 5104.